

Cofactors Involved in Light-Driven Charge Separation in Photosystem I Identified by Subpicosecond Infrared Spectroscopy[†]

Mariangela Di Donato,* Andreas D. Stahl, Ivo H. M. van Stokkum, Rienk van Grondelle, and Marie-Louise Groot

Faculty of Sciences, Department of Physics and Astronomy, VU University Amsterdam, Amsterdam, The Netherlands

Received September 27, 2010; Revised Manuscript Received December 14, 2010

ABSTRACT: Photosystem I is one of the key players in the conversion of solar energy into chemical energy. While the chlorophyll dimer P₇₀₀ has long been identified as the primary electron donor, the components involved in the primary charge separation process in PSI remain undetermined. Here, we have studied the charge separation dynamics in Photosystem I trimers from *Synechococcus elongatus* by femtosecond vis-pump/mid-infrared-probe spectroscopy upon excitation at 700, 710, and 715 nm. Because of the high specificity of the infrared region for the redox state and small differences in the molecular structure of pigments, we were able to clearly identify specific marker bands indicating chlorophyll (Chl) oxidation. Magnitudes of chlorophyll cation signals are observed to increase faster than the time resolution of the experiment (~0.2 ps) upon both excitation conditions: 700 nm and selective red excitation. Two models, involving either ultrafast charge separation or charge transfer character of the red pigments in PSI, are discussed to explain this observation. A further increase in the magnitudes of cation signals on a subpicosecond time scale (0.8–1 ps) indicates the formation of the primary radical pair. Evolution in the cation region with time constants of 7 and 40 ps reveals the formation of the secondary radical pair, involving a secondary electron donor. Modeling of the data allows us to extract the spectra of the two radical pairs, which have IR signatures consistent with A⁺A₀⁻ and P₇₀₀⁺A₁⁻. We conclude that the cofactor chlorophyll A acts as the primary donor in PSI. The existence of an equilibrium between the two radical pairs we interpret as concerted hole/electron transfer between the pairs of electron donors and acceptors, until after 40 ps, relaxation leads to a full population of the P₇₀₀⁺A₁ radical pair.

Photosystem I (PSI)¹ is a membrane protein involved in the primary processes of oxygenic photosynthesis. Operating in conjunction with Photosystem II (PSII), it collects solar energy and transfers electrons from plastocyanin or cytochrome *c*₆ to ferredoxin and eventually to NADP⁺.

PSI is one of the largest membrane proteins for which a crystal structure has been resolved (1, 2) and consists of 11–13 protein subunits, binding approximately 90–100 chlorophyll pigments. The two largest subunits, denoted PsaA and PsaB, form a heterodimer, which binds most of the core antenna pigments as well as the cofactors of the reaction center (RC), shown in Figure 1. The latter traps the excitation energy collected by the antenna and initiates a series of electron transfer processes giving rise to the formation of a stable charge-separated state.

As in PSII, the reaction center's pigments are symmetrically distributed on the two PsaA and PsaB subunits, but in this case, a growing number of experimental investigations suggest that the

electron transfer reactions can occur along both branches of the RC (3–11, 20).

The dynamics of the energy and electron transfer processes occurring in PSI upon photoexcitation have been studied with a range of time-resolved techniques, but general consensus in the interpretation of the experimental observations has not been achieved (4, 12–23).

Resolving the primary energy and electron transfer kinetics in PSI is very challenging, because in this system the reaction center cannot be isolated from the primary antenna, meaning that time-resolved experiments have to be performed on a system containing ~100 chlorophylls. Despite the large number of pigments contained in PSI, only a limited number of lifetimes have been resolved: a subpicosecond component, one or two picosecond lifetimes, and a longer 20–30 ps component, generally interpreted as the main trapping time (16, 22, 24, 25).

Two main models have been proposed to explain the energy and electron transfer dynamics in PSI: the trap-limited model (19, 21–23) and the transfer to the trap kinetic scheme (15, 16, 25–27). The two interpretations differ in ascribing the rate-limiting step in the dynamics following light absorption either to primary charge separation or to the energy transfer from the equilibrated bulk antenna chlorophylls to the reaction center pigments. The interpretation of the experimental data is still controversial because in PSI the excitation dynamics, such as the energy equilibration among the different antenna pigments and with the reaction center, occur on the same time scale as the

[†]This work was supported by The Netherlands Organization for Scientific Research, via NWO-ALW Grants 816.02.008 and 814.02.015. M.D.D. gratefully acknowledges financial support from HFSP Grant RGP0038/2006.

*To whom correspondence should be addressed. Current address: LENS (European Laboratory for Nonlinear Spectroscopy), via N. Carrara 1, Sesto Fiorentino (FI), Italy. Phone: +39 055 4572483. Fax: +39 055 4572451. E-mail: didonato@lens.unifi.it.

¹Abbreviations: Chl, chlorophyll; PSI, Photosystem I; PSII, Photosystem II; RC, reaction center; RP, radical pair; ES, excited state; SADS, species-associated difference spectra; EADS, evolution-associated difference spectra.

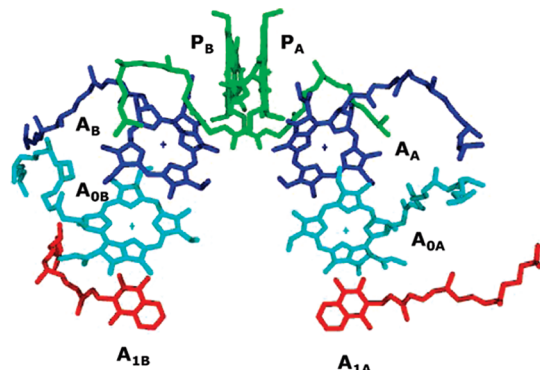


FIGURE 1: Arrangement of the cofactors in the RC from PSI.

primary electron transfer events. It is thus very complicated to disentangle those different processes, unless a clear spectral marker for charge separation is identified. The infrared spectral region can be much more informative in this regard than the visible spectral region, because the oxidation of a chlorophyll pigment, and thus the occurrence of charge separation, is easily identified by the appearance of specific marker bands.

Previous measurements on purple bacterial reaction centers (28–31), PSII-isolated RCs (32), and core samples (33) identified a specific spectral signature for charge separation in the chlorophyll's 9-keto carbonyl absorption region: the carbonyl band, observed around 1680–1700 cm^{-1} in the ground state, shifts upward by 25–30 cm^{-1} upon the localization of the positive charge on the primary donor. In PSI from cyanobacteria, however, a certain number of red-absorbing pigments are present, whose excited state has been shown to have charge transfer character (34, 35). These pigments could thus also have some absorption in the chlorophyll cation region.

The high specificity of the signals in the infrared can lead not only to direct determination of the charge separation time scale but also to the identification of the primary donor, whose precise identity has been recently debated (17, 36). The exact location of an infrared band is highly dependent on the detailed structure of the protein environment around a specific cofactor, thus allowing for distinguishing bands pertaining to the different chlorophylls contained in the system.

On the basis of these premises, we have performed ultrafast time-resolved infrared experiments on PSI with the objective of disentangling the antenna dynamics from the charge separation events, gaining information about both the red-absorbing pigments and the sequence of the electron transfer events in this system.

MATERIALS AND METHODS

Protein Preparation. *Synechococcus elongatus* trimers were isolated as previously described (37). For vis/mid-IR experiments, the sample was concentrated to an OD of ~ 1.0 at 680 nm for a 20 μm optical path length and suspended in 10 mM 2-(*N*-morpholino)ethanesulfonic acid (MES) buffer (pD 7) in D_2O containing 20 mM NaCl, 20 mM MgCl_2 , and 0.05% β -DM. To keep the reaction center open during the measurements, 40 mM sodium ascorbate and 60 μM phenazine methosulfate were added to the sample.

Vis/Mid-IR Pump–Probe. Absorption difference spectra at 67 different time points between -15 ps and 1.8 ns were recorded with a setup based on a 1 kHz amplified laser system described in detail in the Supporting Information. Excitation was

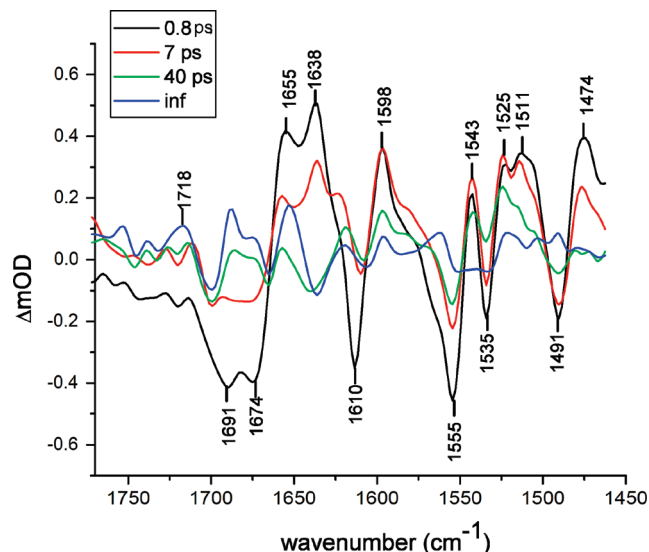


FIGURE 2: EADS estimated by global analysis of the time-resolved data using a sequential kinetic scheme with increasing lifetimes.

set at 700 nm with an excitation power of 100 nJ, and data were collected between 1450 and 1780 cm^{-1} , in two partially overlapping windows (1780–1600 and 1620–1450 cm^{-1}). More than 200 scans were collected and averaged in each spectral window. Furthermore, additional measurements have been performed with selective 710 and 715 nm excitation in the spectral region between 1780 and 1600 cm^{-1} (which includes the range in which chlorophyll's carbonyl absorption is expected), with the excitation power set at 100 nJ. The noise level in the raw data is ~ 70 μOD , which mainly consists of structureless baseline noise because no reference probe pulse has been used.

Data Analysis. The data were subjected to global and target analysis (38); details about the procedure can be found in the Supporting Information.

RESULTS

PSI trimers from *S. elongatus* were excited at 700 nm, and the induced absorption changes were probed in the mid-infrared from -15 ps to 1.8 ns in two partially overlapping windows, covering the spectral region between 1780 and 1450 cm^{-1} . The collected time traces were globally analyzed using a sequential scheme with increasing lifetimes to visualize the dynamics occurring in the system after excitation. Four lifetimes were necessary to obtain a satisfactory fit of the data: 0.8 ps, 7 ps, 40 ps, and a long-lived component with a lifetime longer than 2 ns. The corresponding evolution-associated decay spectra (EADS) are reported in Figure 2. Several time traces are shown in Figure 3, together with the fit resulting from global analysis.

In the EADS, negative bands are due to bleached ground state absorption and positive bands arise from modes in the excited or charge-separated states. Both cofactors and protein modes contribute to the signals, and the spectra appear to be very rich in features.

The initial difference spectrum, with a subpicosecond lifetime, mainly represents the excited state of the antenna chlorophylls, which, according to previous studies (17, 22, 36), rapidly equilibrates after excitation. Several modes previously assigned to chlorophyll molecules can be identified in this spectral component. In the higher-wavenumber region, approximately between 1650 and 1750 cm^{-1} , carbonyl modes are expected. Accordingly,

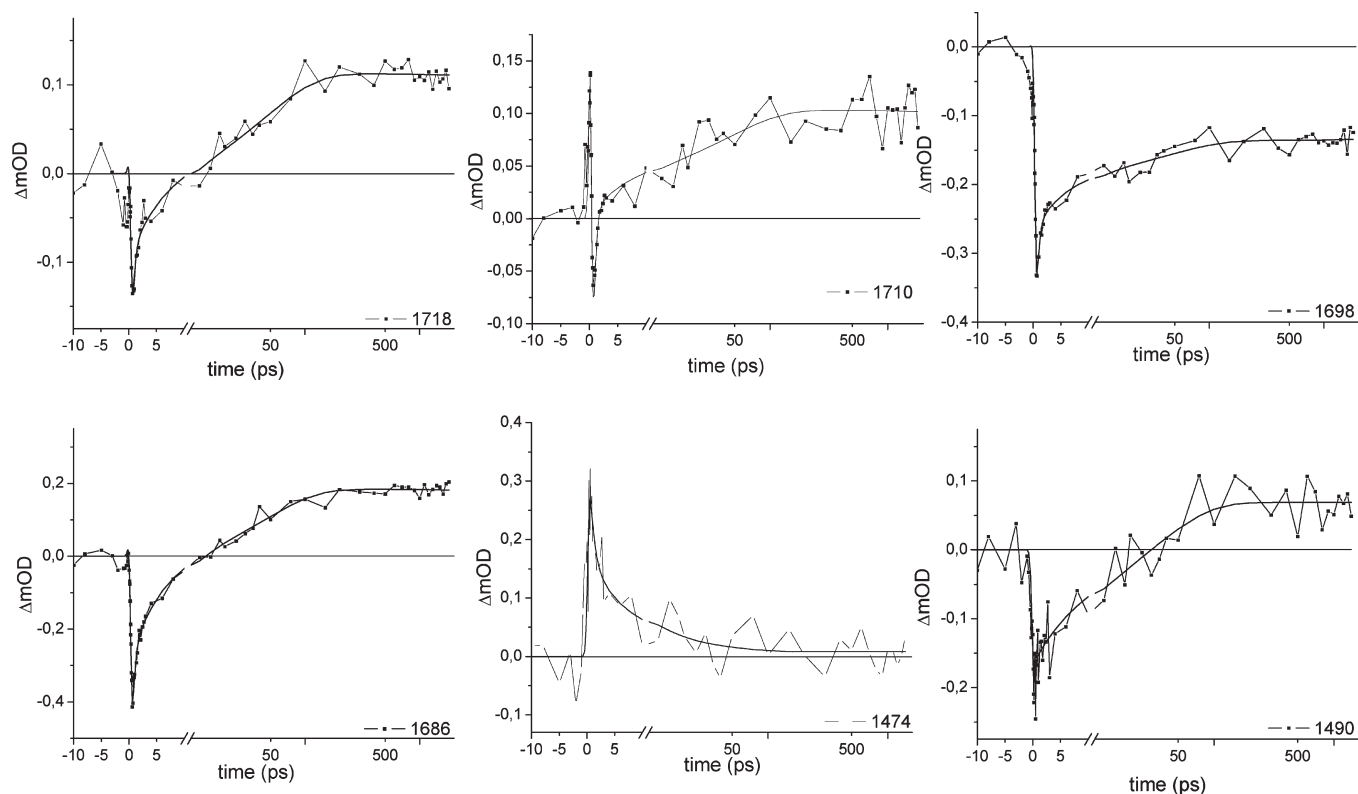


FIGURE 3: Selected time traces measured in the infrared (1780–1450 cm^{-1}) by exciting PSI trimers from *Synechococcus* at 700 nm and relative fit (—) obtained via global analysis of the time-resolved data. The time scale of the plot is linear up to 10 ps and logarithmic from 10 ps to 2 ns.

an intense bleaching feature peaking at 1691 and 1674 cm^{-1} is observed, representing the ground state absorption of the 9-keto groups of chlorophylls located in different environments. The chlorophyll's carbonyl bands are very sensitive to their surroundings, and downshifts larger than 20 cm^{-1} can be expected with respect to the frequency observed in nonpolar solvents (i.e., 1695 cm^{-1} in THF) (39), because of the presence of hydrogen bonds or differences in the polarity of the surrounding medium. The bleach at approximately 1740–1750 cm^{-1} can be assigned to 10a-ester absorption. In the excited state, both 9-keto carbonyl and 10a-ester bands downshift by several wavenumbers (32, 40, 41). The intense band peaking at 1655 and 1638 cm^{-1} can be thus assigned to the downshifted keto carbonyl of chlorophylls in the excited state.

In the lower-wavenumber region, the bands at 1610 and 1555 cm^{-1} have been assigned to chlorophyll macrocycle modes (42) and are indicative of pentacoordination of the chlorophyll ring. The bleach at 1535 cm^{-1} could also be a chlorophyll ring mode [observed at 1527 cm^{-1} in vitro (39)]. All those bands are expected to downshift because of the reduced bond order in the excited state, giving rise to the positive features observed at 1543 and 1511 cm^{-1} . Protein modes also absorb in this region, and contributions of amide I and II bands may be expected around 1650 and 1550 cm^{-1} (43).

After 0.8 ps, the system evolves to the second EADS, reported as a red line in Figure 2. Here we observe a substantial decay of the positive excited state bands, especially in the C=O region (around 1650 cm^{-1}) indicating quenching of the antenna excited state due to energy transfer and equilibration with the reaction center. Because of the relatively high excitation intensity used in our experiment, annihilation processes resulting from multiple excitations in a single complex accelerate the excited state decay as well. In the 1715 cm^{-1} region, several positive features appear, and the position of these bands corresponds well with the

upshifted chlorophyll keto carbonyl bands due to oxidation (32, 33, 44–46). The appearance of these positive bands indicates subpicosecond Chl^+ formation. Note that these bands are partially present already in the first EADS.

The absorption difference spectra then evolve in ~ 7 ps into the following component, represented by the green line in Figure 2, which shows a complete decay of all the excited state features and the appearance of a new bleaching around 1645 cm^{-1} . Finally, after ~ 40 ps, the final spectral component is formed. This spectrum is characterized by distinctly different spectral features, among others in the region of the Chl cation around 1715 cm^{-1} , where the double band transforms into a single band, and the appearance of positive bands at 1680 and 1653 cm^{-1} . This component should represent the final charge-separated state reached by the system under our measuring conditions, namely $\text{P}_{700}^+\text{A}_1^-$, where P_{700} is the chlorophyll dimer contained in PSI and A_1 is a phylloquinone molecule.

DISCUSSION

The time-resolved mid-IR absorption difference spectra show several interesting features, e.g., the ultrafast appearance of a chlorophyll cation band, the evolution in the cation region, possibly suggesting the involvement of different electron donors, and the appearance of A_1 bands. In the following, we will discuss these observations in more detail.

Ultrafast Charge Separation or Charge Transfer?. The EADS rising in 0.8 ps and, to a minor extent, the initial EADS show characteristic spectral features that are indicative of chlorophyll oxidation, which can be attributed either to the presence of excited states with charge transfer character or to charge separation occurring on a subpicosecond time scale. Charge separation in PSI has recently been proposed to be ultrafast (based on the

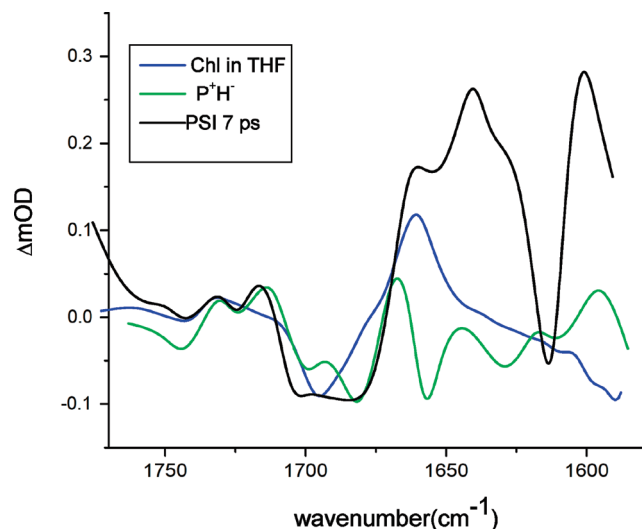


FIGURE 4: Comparison of the 7 ps spectral component estimated by a global analysis of the time-resolved data collected for PSI (black line) with the time-resolved spectrum of the charge-separated state P^+H^- measured in PSII RCs from spinach (32) in the carbonyl absorption region, where P denotes the special pair electron donor and H the pheophytin acceptor in PSII. Furthermore, the absorption difference spectrum of chlorophyll *a* in the excited state is reported, recorded 10 ps after excitation at 530 nm in THF (32).

fast appearance of a Chl^- signal in visible pump–probe measurements) (47), and at first sight, our observations seem to support this suggestion. Figure 4 shows the overlay of the second EADS reported in Figure 2 with the infrared time-resolved spectrum of the P^+H^- charge-separated state measured in PSII RCs from spinach (32) in the carbonyl absorption region, where P denotes the special pair electron donor and H the pheophytin acceptor in PSII. Furthermore, the absorption difference spectrum of chlorophyll *a* in the excited state is reported, recorded 10 ps after excitation at 530 nm in THF (32).

The spectrum of chlorophyll *a* clearly shows the downshift of the 9-keto and 10a-ester carbonyls in the excited state, whose vibrational frequency shifts from 1695 to 1660 cm^{-1} and from 1740 to 1730 cm^{-1} , respectively. The green spectrum, representing the time-resolved charge-separated P^+H^- spectrum measured in PSII RCs (32), shows a pronounced double-peak feature with maxima at 1715 and 1730 cm^{-1} , which have been attributed to the localization of a positive charge on a chlorophyll dimer (48). The same double-peak band is present in the radical pair spectra measured for PSII core particles and bacterial reaction centers (29, 33, 49). Less than 1 ps after excitation, a double-peak absorption in the 1715 cm^{-1} region also develops in PSI, whose EADS, after a 3 cm^{-1} upshift on the wavelength axis, coincides very well with those previously reported for the charge-separated state of PSII RCs. The comparison reported in Figure 4 thus strongly suggests that chlorophyll cations are formed on a subpicosecond time scale in PSI.

The EADS, like those shown in Figure 2, are not pure spectra, representing only one intermediate state, but represent mixtures of excited state spectra and radical pair spectra. It is well-known that cyanobacterial PSI systems, and in particular the *Synechococcus* particles used in this study, contain a certain number of red antenna pigments, absorbing at wavelengths higher than 700 nm, apart from the more blue-absorbing bulk pigments. Although the nature and the exact function of those red pigments is still under debate, several investigations suggest that those red pigments form strongly interacting chlorophyll dimers or trimers and that their excited states have substantial charge transfer character (34, 35).

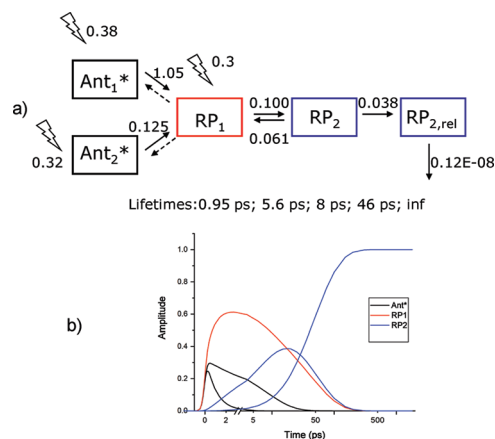


FIGURE 5: (a) Kinetic model 1 used for the target analysis of time-resolved data. The rate constants (in ps^{-1}), lifetimes (in ps), and input values on the initially populated compartments are reported. (b) Concentration profile of the time-dependent population of the five compartments used in the kinetic scheme.

Therefore, the cation signature observed in the first two EADS may also arise from the charge transfer character of these red chlorophylls. To understand the nature of the signal observed in the Chl cation region, we performed a target analysis based on specific kinetic models that aimed to disentangle the contributions of bulk excited state antennas, red chlorophylls, and radical pair states.

Simple Kinetic Scheme for Target Analysis (model 1). Inspection of the EADS reported in Figure 2 shows that the antenna's dynamics is heterogeneous and that two excited state compartments are necessary to describe the biphasic decay of the excited state signal around 1650 cm^{-1} . Furthermore, several features in the green EADS appear as a combination of the red and blue spectra, thus suggesting the presence of two radical pair states in an equilibrium. As a starting point for the analysis, we have used a simple kinetic scheme, whose main intent is to separate as much as possible antenna and radical pair contributions. The kinetic scheme is reported in Figure 5, together with the rate constants (in ps^{-1}), estimated when this model is fit to the data, and the concentration profiles of the resolved intermediates.

The scheme reported in Figure 5 consists of five compartments: two excited state compartments and three radical pair compartments, two of which are in equilibrium with each other. Compared with other kinetic schemes reported in the literature, as for instance in refs 11, 17, and 19, this is a very simplified model; nevertheless, it allows the extraction of important information from the data. The SADS (species-associated decay spectra) estimated by fitting the data using the kinetic scheme of Figure 5 are reported in Figure 6.

The SADS of the two excited state compartments are imposed to be spectrally identical, as well as those of the second and third radical pairs, giving rise to only three distinct spectra for the five compartments (for a more detailed discussion of the target modeling, see the Supporting Information). The obtained SADS are reasonable. Using this model, all the positive features in the 1710–1730 cm^{-1} region indicating chlorophyll oxidation are interpreted as indicating radical pair formation and are removed from the antenna spectra by allowing for 30% direct excitation in the first RP compartment.

The excited state SADS include all the spectral features previously discussed, and assigned to chlorophyll excited states, but no distinction is made between red and bulk antenna chlorophylls.

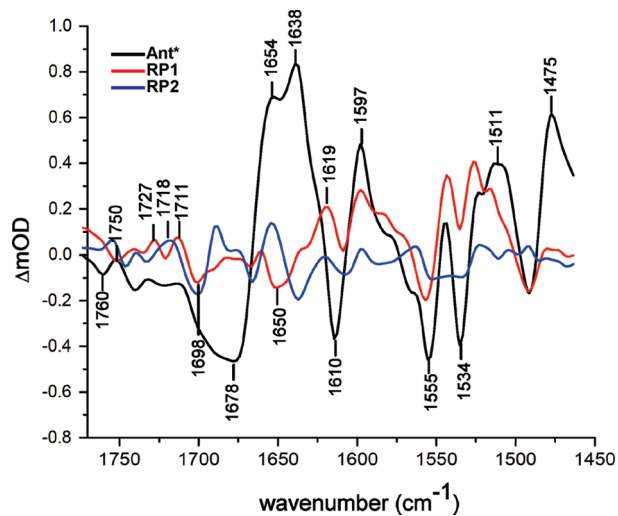


FIGURE 6: SADS obtained by applying the kinetic scheme reported in Figure 5a to the time-resolved data. Spectra of $\text{Ant}^*_1 = \text{Ant}^*_2$ (black line), RP1 (red line), and $\text{RP2} = \text{RP2}_{\text{rel}}$ (blue line).

The next two SADS are free of excited state features, show distinct signals that can be attributed to cation and anion states, and can therefore be interpreted as radical pair spectra. However, as they are dissimilar, we have to conclude that different cofactors are involved in those intermediates. The $\text{RP2} = \text{RP2}_{\text{rel}}$ SADS, which are, as expected, spectrally identical to the final EADS obtained with the sequential analysis, represent the final state reached by the system, $\text{P}_{700}^+ \text{A}_1^-$. A more detailed discussion of the RP2 spectrum and a comparison with the FTIR spectrum of P_{700}^+ are given at the end of this section.

According to this model, the electron transfer rates lead to an equilibrium between the two radical pair states, established in ~ 6 ps. A relaxation in RP2 [possibly a decrease in the free energy ΔG , as observed for other RCs (29, 50, 51)] after 46 ps leads to a decay of this equilibrium and a localization of the electron on A_1 . The subsequent electron transfer processes occur on a time scale of hundreds of nanoseconds, beyond our time window (4).

The differences between RP1 and RP2 in the $1730\text{--}1710\text{ cm}^{-1}$ region may suggest the involvement of another Chl donor, too, as this region is dominated by Chl cation absorption (28, 48, 52). However, before we discuss the nature and assignment of the bands in each radical pair in more detail, we will first develop two more advanced models to test whether we can describe RP formation and the dynamics associated with the red pigments in PSI in more detail.

Charge Separation and Reversible Energy Transfer (model 2). The target model of Figure 5 (model 1) seizes the essential dynamics of the system in a very simple way, but it imposes severe approximations in the modeling of the system's dynamics. First, this model does not include a separate compartment for the excited state of the reaction center or a separate red chlorophyll compartment. Because the excitation wavelength of 700 nm is resonant with some of the RC pigments, by assuming a relative oscillator strength of two RC Chls at 700 nm, we estimate that 30% of the photons directly excite the RC (see the Supporting Information). Modeling these excitations as feeding directly into RP1, as in model 1, suggests that the charge separation, once the excitation is at the 700 nm-absorbing pigments located in the

RC, is ultrafast. Within the simple model 1, the transfer of energy from the antenna to the reaction center appears to be almost unidirectional (backward rates, if introduced in the scheme of model 1, are ~ 10 -fold smaller than forward rates), while physically more reasonable schemes, like those used to model time-resolved fluorescence or visible pump–probe experiments (17, 36), include reversible energy and electron transfer processes.

Inspection of equilibrium models (11, 17, 21) reveals that the equilibrium between Ant^* and RC^* is shifted toward the antenna state, because of the high number of chlorophyll molecules contained in the antenna, and that the equilibrium between RC^* and RP1 is shifted toward the RP1 state because of the fast charge separation rate. These considerations suggest that the inclusion of RC^* dynamics in the antenna compartment can result in an almost irreversible RP1 formation, similar to what we found here.

To test this hypothesis, we designed a model that included an extra excited state (ES) compartment denoted “700*”, from which charge separation occurs. This state should include all the pigments with significant absorption at 700 nm; therefore, besides P_{700} , some of the antenna pigments and possibly also the reaction center's chlorophylls A and A_0 are included. The scheme is shown in Figure 7, together with the rate constants (in ps^{-1}), estimated when this model is fit to the data and the concentration profiles of the compartments. The corresponding SADS are shown in Figure 8.

With a charge separation rate of 3 ps^{-1} , we find that it is now indeed possible to introduce reversibility in the energy transfer processes. Radical pair formation is modeled as irreversible, and attempts to set a back transfer toward the 700* compartment indicate that, within the frame of this model, the amount of charge recombination cannot be higher than 10%, to prevent spectral compensation and distortion in the SADS.

The SADS of the three excited state compartments are imposed to be identical, so it is not possible to identify specific spectral signatures of the red chlorophylls, if any are present. Energy can be transferred from both the “Bulk*” and “Red*” compartments toward the 700* compartment. The slowly transferring Red* ES compartment is not connected with 700* but only with the other ES. The omission of direct connection among the two compartments is of course an approximation, which, however, we expect to have a minor effect on the dynamics. There are several reports in the literature suggesting that P_{700} and Red* do not equilibrate on a fast time scale. For instance, low-temperature fluorescence measurements on *S. elongatus* showed that bulk excitation at 4 K leads to 50% of the excitations ending in the red pigments and 50% in the radical pair state (53). This implies that P_{700} and Red* are not strongly connected, possibly because of their spatial location.

The equilibrium now introduced into the excited state is on the Bulk* compartment, in agreement with the large number of pigments that this state represents. According to our estimate, as a result of the back transfer, more than half of the excitations rapidly escape from the reaction center.

With regard to the antenna dynamics, we note that our experiments suffer from a significant amount of excitation annihilation, because of the presence of multiple excitations in the system (cf. the ~ 3 -fold lower signals after 7 ps in Figure 2 or of the RP spectra relative to those of the ES compartments). This leads to an underestimation of the backward to forward rate ratio; therefore, the numbers reported in Figure 7 should be interpreted with some care. Inspection of the concentration profiles reported in Figures 5 and 6 and of the EADS reported

²This notation indicates that two compartments RP2 and RP2_{rel} (which stands for RP2 relaxed) are imposed to be spectrally identical.

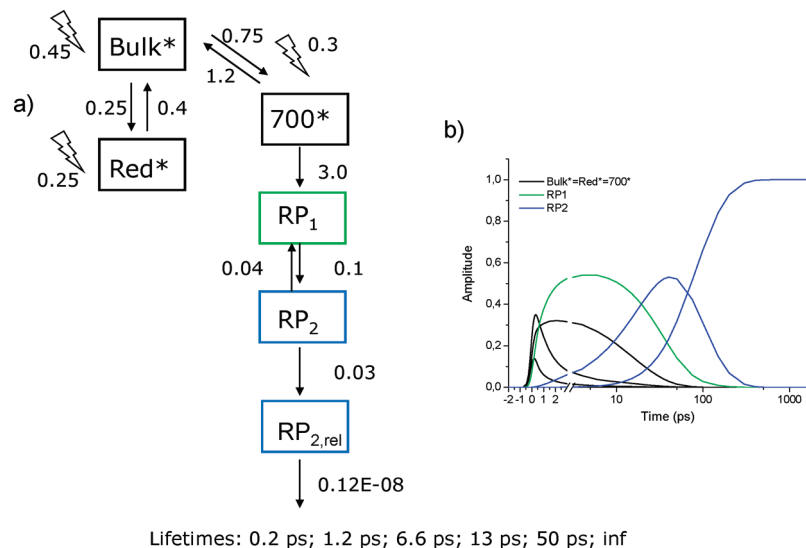


FIGURE 7: (a) Kinetic model 2 used for the target analysis of time-resolved data. The rate constants (in ps^{-1}), lifetimes (in ps), and input values on the initially populated compartments are reported. (b) Concentration profile of the time-dependent population of the five compartments used in the kinetic scheme.

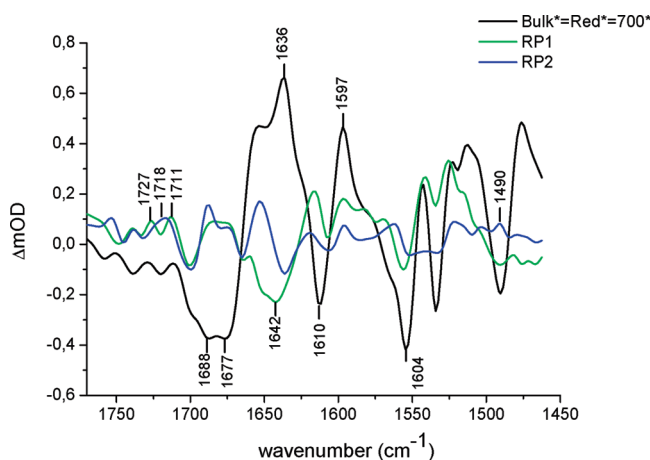


FIGURE 8: SADS obtained by applying the kinetic scheme reported in Figure 7a to the time-resolved data. Spectra of Bulk*+700*=Red* (black line), RP₁ (green line), and RP₂=RP_{2,rel} (blue line).

in Figure 2 shows that in our experiment, the excited states substantially decay on a 10 ps time scale, faster than previously reported (54). Previous fluorescence and visible pump–probe measurements indeed indicated a slower trapping dynamics with a main trapping time of approximately 30–35 ps, due to the participation of the red pigments in the equilibrated excited state (15, 19, 55). As a rough estimate, considering that having n excitations per center leads to an n -fold decrease in the trapping time (55), it has to be concluded that in our measurements we have at least three excitations per center. Besides that, selective 700 nm excitation could also contribute to fastening the antennas' excited state decay. Time-resolved fluorescence measurements with 700 nm excitation on *Synechocystis* or 710 nm on *Synechococcus* samples showed in fact the presence of a fast (< 1 ps) energy transfer component and a 10–13 ps decay component, not observed upon nonselective excitation, which was mainly ascribed to non-equilibrium trapping (26). The combination of annihilation between multiple excitations in the antenna and quenching from the directly formed (nonequilibrium) charge-separated state upon specific RC excitation, taking place simultaneously, determines the faster antenna decay observed in our measurements.

In the framework of this model (model 2), all the spectral features growing in with the sub-10 ps time constants, and decaying in 40 ps, are described by the spectrum of RP₁. As mentioned earlier, one of the limitations due to the spectral constraints imposed in this model is the impossibility of discerning any specific signature of the red pigments. Therefore, we pose the following question. Is it possible that part of the early cation features are in fact coming from the red chlorophylls in PSI, which after all, have been reported to have charge transfer character (56)? To address this issue, we modified target model 2 and allowed the SADS of Red* to be different from those of Bulk* and 700* (model 3).

Red Chlorophylls. With the release of the spectral constraint on the Red* SADS, the same kinetic scheme reported in Figure 7 allows for the determination of a specific SADS representing the excited state of red chlorophylls. The kinetic scheme together with the rate constants (in ps^{-1}), which are as expected not very different from those obtained with model 2, and the concentration profiles of the compartments are reported in Figure 9, while the corresponding SADS are shown in Figure 10.

The SADS we obtain for the red chlorophyll compartment (red line in Figure 10) has a pronounced positive band at 1710 cm^{-1} , showing that, according to this model, the early cation features are mostly associated with the red Chls. This may be a result of a significant charge transfer character for this excited state. In comparison to the black SADS, representing the excited state of bulk and 700 nm-absorbing pigments, the carbonyl excited state absorption band is downshifted, possibly partly because of the mixing with anion bands [expected at ~ 1600 cm^{-1} (45)] that are the counterparts for the 1710 cm^{-1} cation absorption.

To gather more information about the absorption spectrum of the red chlorophylls in the IR, we performed additional time-resolved experiments using selective excitation wavelengths (more details can be found in the Supporting Information).

The excited state spectra (i.e., initial EADS with a lifetime of ~ 1 ps) obtained when using excitation wavelengths of 710 and 715 nm show several features that are similar to those observed in the red SADS reported in Figure 10; a spectral overlay is reported in Figure 11.

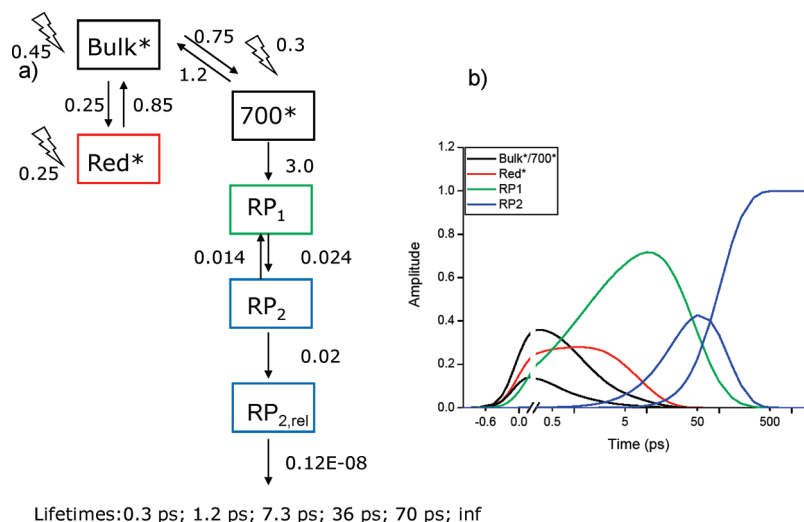


FIGURE 9: (a) Kinetic model 3 used for the target analysis of time-resolved data. The rate constants (in ps^{-1}), lifetimes (in ps), and input values on the initially populated compartments are reported. (b) Concentration profile of the time-dependent population of the five compartments used in the kinetic scheme.

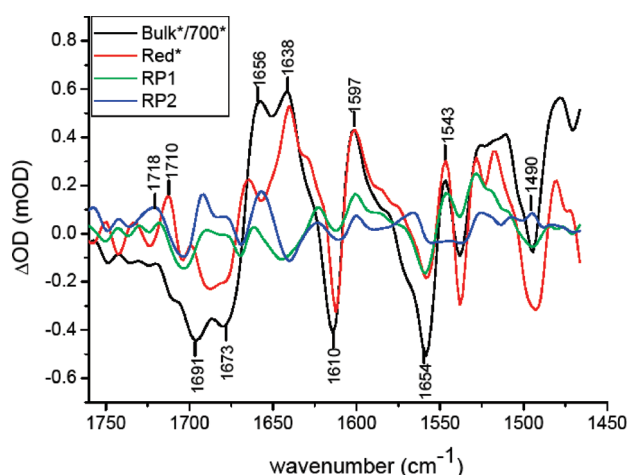


FIGURE 10: SADS obtained by applying the kinetic scheme reported in Figure 9a to the time-resolved data. Spectra of Bulk* = 700* (black line), Red* (red line), RP1 (green line), and RP2 = RP_{2,rel} (blue line).

Therefore, it appears that the spectrum of the compartment labeled Red* in model 3 indeed represents the red pigments of PSI. All three spectra reported in Figure 11 have a pronounced absorption band at 1710 cm^{-1} , although the shape and maximum of the excited state absorption band ($\sim 1635\text{ cm}^{-1}$) appear to be wavelength-dependent. The presence of bands consistent with cation or anion modes of chlorophyll pigments in the excited state spectrum of the red Chls in PSI may be explained by the excited state of the red pigments having a significant charge transfer character.

We note, however, that until now IR-difference spectra have, to the best of our knowledge, not yielded indications of cation–anion contributions in other systems with confirmed CT mixed excited state character. For instance, in the case of protochlorophyllide in solution, charge transfer states were shown to be mixed with the excited states both, experimentally, by a full quenching of the emission during the excited state lifetime and by time-dependent DFT calculations (57), and similarly for a carotenoid chromophore in the OCP protein (58), but no indicative cation features were identified in the IR difference spectra of these systems. Therefore, it is not a priori expected that a

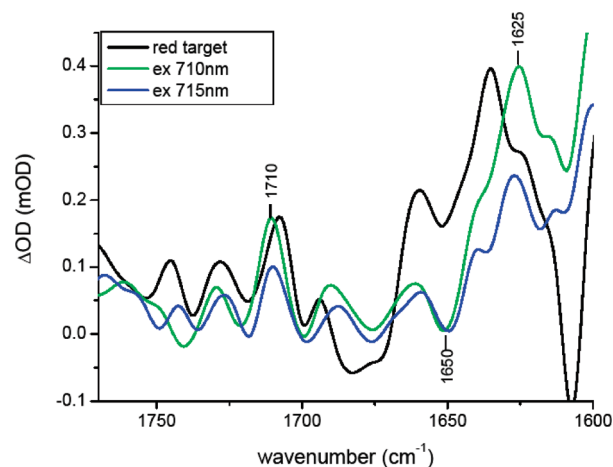


FIGURE 11: Comparison between the red chlorophyll SADS obtained by applying target model 3 to the time-resolved data collected for PSI upon 700 nm excitation (black line) with the time-resolved spectrum measured 1 ps after excitation using selective wavelengths for excitation of red chlorophylls at 710 nm (green line) and 715 nm (blue line).

charge transfer character of the red states would manifest itself as cation and anion features in the IR spectra.

An alternative explanation for early cation features in the spectra registered upon 710 and 715 nm excitation is that RP formation is very fast even upon red excitation, leading to a mixture of RP1 and red excited states in the first spectral component. The possibility of charge separation occurring upon far red excitation has been also discussed in the case of PSII (59). If confirmed, this would be a general characteristic of both photosystems, with important implications concerning the way in which the photosynthetic machinery has evolved to optimize its operation. Experiments with a form of PSI without red pigments are necessary to determine which of these two explanations is correct.

Nature of RP1 and RP2. The SADS obtained for the two radical pair states depend to a certain extent on the kinetic scheme used. When the simple model 1 or model 2 is applied, the two radical pair SADS present more distinctive features than those in model 3. However, all models show that upon formation of RP2

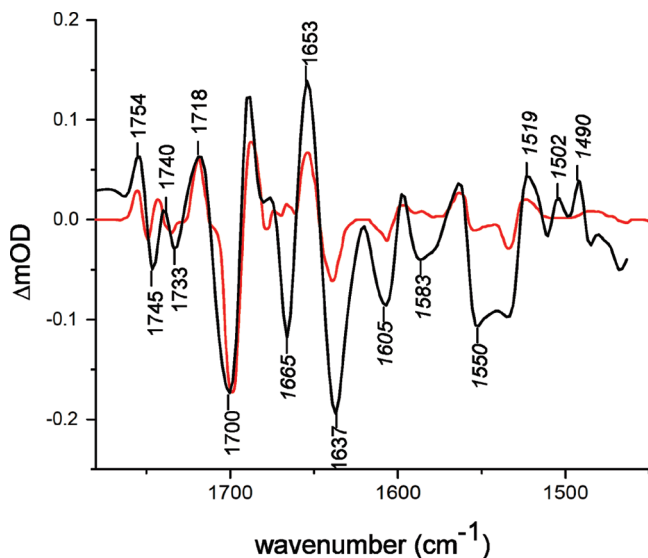


FIGURE 12: Comparison between the RP2 = RP2_{rel} SADS obtained by target analysis and the light-induced FTIR P₇₀₀⁺/P₇₀₀ spectrum measured in PSI. The FTIR spectrum has been obtained by digitizing Figure 1A of ref 52. The two spectra have been normalized with respect to the intensity of the P_B⁺/P_B signals [1700(-)/1718(+) cm^{-1}].

from RP1, an evolution both in the anion region, where some spectral features attributable to the formation of a semiquinone appear, and in the cation region occurs. The kinetic evolution in the $> 1700\text{ cm}^{-1}$ region can be noticed also via inspection of the time traces reported in Figure 3. By comparing the kinetics at 1710 cm^{-1} with that at 1718 cm^{-1} (assigned to the C=O group of P_B⁺), (56) we can notice that while the first time trace increases immediately after time zero, the 1718 cm^{-1} time trace becomes positive only several picoseconds after excitation. Therefore, we conclude that our findings are in line with recent interpretations of visible pump-probe experiments suggesting the primary radical pair is A⁺A₀⁻ and not P₇₀₀⁺A₀⁻ (17, 36). The possibility of an alternative pathway for charge separation not involving the special pair had been suggested in the case of bacterial reaction centers (60, 61). Furthermore, also in the reaction center of PSII, the accessory Chl has been identified as an electron donor (32, 62). Once again, this finding has implications with regard to the optimization of natural photosynthetic systems. It is possible in fact that starting the charge separation process at the Chl monomer site and then rapidly creating a secondary radical pair involving P₇₀₀ reduces the possibility of charge recombination with respect to the situation in which subsequent electron transfers are involved, as would happen with P₇₀₀ as the primary donor.

The assignments of the bands in the RP1 spectrum to the IR modes of the involved pigments can be found in the Supporting Information.

Final Spectral Component: A₁⁻/A₁ Bands. The final spectral component is identical regardless of the kinetic model applied to the data and also coincides with the final EADS obtained by using a sequential scheme (shown in Figure 2). To verify that indeed the final state reached by the system is P₇₀₀⁺A₁⁻, we have compared in Figure 12 the nondecaying component obtained in our measurements with the P₇₀₀⁺/P₇₀₀ light-induced FTIR spectrum, which has been previously reported in the literature (52).

Besides the bands previously assigned to P₇₀₀, which agree very well with those measured by FTIR, the time-resolved spectrum shows further features, some of which can be assigned to A₁⁻. The bands at $1700(-)/1718(+)$ and $1637(-)/1653(+)\text{ cm}^{-1}$ have

been assigned by FTIR measurements to the 9-keto carbonyls of the two P_B and P_A chlorophylls forming P₇₀₀ and the bands at $1745(-)/1754(+)$ and $1733(-)/1740(+)\text{ cm}^{-1}$ to the corresponding 10a-ester groups (52). With regard to the quinone's bands, a comparison is possible with a previously reported time-resolved P₇₀₀⁺A₁⁻ spectrum, measured at 77 K using time-resolved step-scan FTIR at $5\text{ }\mu\text{s}$ resolution (63), which agrees well with that reported in Figure 12.³ We note that there is a difference in the relative intensity of the bands at $1700(-)/1718(+)$ and $1637(-)/1653(+)\text{ cm}^{-1}$ between the FTIR spectrum and all the time-resolved spectra, both the one displayed in Figure 12 and those reported in ref 63. In all the time-resolved spectra, the band at $1637(-)/1653(+)\text{ cm}^{-1}$ is more intense than in the FTIR spectrum. A higher intensity of a differential band in the amide region is also reported in the case of time-resolved IR spectra of PSII as compared with the corresponding static FTIR spectra (64). This finding is possibly due to an environmental effect and to the possibility that the protein is not in a fully relaxed conformation on the time scale of the time-resolved experiments. Further insights into the assignment of A₁ modes can be obtained from the comparison of the RP2 SADS with the electrogenerated spectrum of vitamin K₁ films, where three main absorption bands at 1661 (C=O) , $1621\text{ (quinoid C=C)}$, and $1596\text{ (aromatic C=C)}\text{ cm}^{-1}$ have been identified (65). On that basis, we can tentatively assign the band at 1665 cm^{-1} (besides amide I contributions) to the C=O stretching mode and the band at 1583 cm^{-1} either to the quinoid C=C stretching or to the aromatic C=C stretching of A₁. The downshift of the C=C quinoid and/or aromatic bands in PSI with respect to what measured for vitamin K₁ films (from $1621/1596$ to 1583 cm^{-1}) is possibly due to the presence of TrpA697, whose aromatic ring is π -stacked on top of the quinone ring (1, 2). In addition, the crystal structure of PSII shows that the two C=O carbonyls of A₁ are not equally coordinated, because only one of them is engaged in a hydrogen bond. This could determine the splitting of the symmetric and antisymmetric C=O vibrations into two localized modes; one of them (that pertaining to the H-bonded C=O group) is downshifted and possibly contributes to the 1605 cm^{-1} band. Such a large downshift for a quinone's C=O vibration has been reported for the Q_A cofactor of purple bacterial reaction centers, where due to a strong hydrogen bond interaction with residue HisM219, the C=O mode downshifts at 1601 cm^{-1} (66). All the quinone bands downshift in the anion state, most likely giving rise to the positive bands at 1502 and 1490 cm^{-1} (corresponding bands in vitro are found at 1536 and 1488 cm^{-1} , respectively).

Final Kinetics Considerations. In all models, the intrinsic initial charge separation is very fast (3 ps^{-1}), forming A⁺A₀⁻. In addition, the secondary electron transfer step, leading to reduction of quinone cofactor A₁, is faster than previously reported: the models consistently show that in $\sim 6\text{ ps}$ an equilibrium between A⁺A₀⁻ and P₇₀₀⁺A₁⁻ is formed. After 40 ps, this equilibrium shifts toward a full population of P₇₀₀⁺A₁⁻. The time constant of 40 ps is in good agreement with literature reports (4). However, the intrinsic rate of reduction of A₁ is now resolved to be $(6\text{ ps})^{-1}$, because of the high specificity of the A₁⁻/A₁ signals in the mid-IR. This makes the reduction of the quinone in PSI not 1 but 2 orders of magnitude

³In discussing quinone-band assignments, we remark that here, for the sake of simplicity, we refer only to the quinone located in the A branch of PSI, treating the electron transfer as unidirectional, although recently support for bidirectionality has been provided (11). Further and more accurate analysis is necessary to evaluate the degree of bidirectionality in the process.

faster than those of reoxidation of Pheo_A⁻ by Q_A in type II RCs (see also ref 67).

CONCLUSIONS

We performed time-resolved infrared experiments on PSI from *S. elongatus* with open reaction centers to provide insights into the charge separation dynamics of this system. The high specificity of infrared bands allowed for recognition of specific spectral signatures due to chlorophyll and quinone oxidation and reduction. Three kinetic models of increasing complexity have been used to analyze the data. The data show very early cation features, which can be interpreted either as ultrafast (< 0.3 ps) charge separation (in models 1 and 2) or as the signature of a charge transfer character of the red pigments contained in PSI (model 3). The former would imply that primary radical pair formation occurs also under far red excitation, which has been suggested to occur in PSII, too (59).

Irrespective of this ambiguity, the data show that charge separation, once the excitation reaches the RC, is ultrafast, occurring with an effective rate constant of 1 ps⁻¹ (intrinsic rate of 3 ps⁻¹). Spectral evolution in the cation region provides strong support for the thesis that in PSI charge separation is initiated at the monomer chlorophyll A, not at P₇₀₀. The specific signature of phylloquinone A₁ in the mid-IR allowed us to determine the reduction of A₁ occurs with an intrinsic time constant of 6 ps. Initially, an equilibrium between A⁺A₀⁻ and P₇₀₀⁺A₁⁻ exists, which relaxes, leading to a full population of the P₇₀₀⁺A₁⁻ state after 40 ps. We provided a full band assignment for the resolved radical pair states, in line with structural data and the published FTIR spectra of electrogenerated vitamin K₁ anion.

ACKNOWLEDGMENT

We thank H. Fidder and K. Heyne for providing the sample.

SUPPORTING INFORMATION AVAILABLE

More detailed description of the experimental setup, selected kinetic time traces, description of the kinetic models used for target analysis, and EADS measured upon excitation with 710 and 715 nm laser pulses. This material is available free of charge via the Internet at <http://pubs.acs.org>.

REFERENCES

- Fromme, P., Jordan, P., and Krauss, N. (2001) Structure of photosystem I. *Biochim. Biophys. Acta* 1507, 5–31.
- Jordan, P., Fromme, P., Witt, H. T., Klukas, O., Saenger, W., and Krausz, N. (2001) Three-dimensional structure of cyanobacterial photosystem I at 2.5 Å resolution. *Nature* 411, 909–917.
- Ali, K., Santabarbara, S., Heathcote, P., Evans, M. C. W., and Purton, S. (2006) Bidirectional electron transfer in photosystem I: Replacement of the symmetry-breaking tryptophan close to the PsaB-bound phylloquinone (A1B) with a glycine residue alters the redox properties of A1B and blocks forward electron transfer at cryogenic temperatures. *Biochim. Biophys. Acta* 1757, 1623–1633.
- Brettel, K., and Leibl, W. (2001) Electron transfer in photosystem I. *Biochim. Biophys. Acta* 1507, 100–114.
- Dashdorj, N., Xu, W., Cohen, R. O., Golbeck, J. H., and Savikhin, S. (2005) Asymmetric Electron Transfer in Cyanobacterial Photosystem I: Charge Separation and Secondary Electron Transfer Dynamics of Mutations Near the Primary Electron Acceptor A0. *Biophys. J.* 88, 1238–1249.
- Fairclough, W. V., Forsyth, A., Evans, M. C. W., Rigby, S. E. J., Purton, S., and Heathcote, P. (2003) Bidirectional electron transfer in photosystem I: Electron transfer on the PsaA side is not essential for phototrophic growth in *Chlamydomonas*. *Biochim. Biophys. Acta* 1606, 43–55.
- Guergova-Kuras, M., Boudreaux, B., Joliot, A., Joliot, P., and Redding, K. (2001) Evidence for two active branches for electron transfer in photosystem I. *Proc. Natl. Acad. Sci. U.S.A.* 98, 4437–4442.
- Ivashin, N., and Larsson, S. (2003) Electron transfer pathways in photosystem I reaction centers. *Chem. Phys. Lett.* 375, 383–387.
- Poluektov, O. G., Paschenko, S. V., Utschig, L. M., Lakshmi, K. V., and Thurnauer, M. C. (2005) Bidirectional Electron Transfer in Photosystem I: Direct Evidence from High-Frequency Time-Resolved EPR Spectroscopy. *J. Am. Chem. Soc.* 127, 11910–11911.
- Xu, W., Chitnis, P. R., Valieva, A., van der Est, A., Brettel, K., Guergova-Kuras, M., Pushkar, Y. N., Zech, S. G., Stehlik, D., Shen, G., Zybailov, B., and Golbeck, J. H. (2003) Electron Transfer in Cyanobacterial Photosystem I: II. Determination of forward electron transfer rates of site-directed mutants in a putative electron transfer pathway from A0 through A1 to Fx. *J. Biol. Chem.* 278, 27876–27887.
- Müller, M. G., Slavov, C., Luthra, R., Redding, K. E., and Holzwarth, A. R. (2010) Independent initiation of primary electron transfer in the two branches of the photosystem I reaction center. *Proc. Natl. Acad. Sci. U.S.A.* 107, 4123–4128.
- Hastings, G., Reed, L. J., Lin, S., and Blankenship, R. E. (1995) Excited state dynamics in photosystem I: Effects of detergent and excitation wavelength. *Biophys. J.* 69, 2044–2055.
- Bender, S. L., and Barry, B. A. (2008) Light-Induced Dynamics in Photosystem I Electron Transfer. *Biophys. J.* 95, 3927–3934.
- Damjanovic, A., Vaswani, H. M., Fromme, P., and Fleming, G. R. (2002) Chlorophyll Excitations in Photosystem I of *Synechococcus elongatus*. *J. Phys. Chem. B* 106, 10251–10262.
- Gobets, B., and van Grondelle, R. (2001) Energy transfer and trapping in photosystem I. *Biochim. Biophys. Acta* 1507, 80–99.
- Gobets, B., van Stokkum, I. H. M., Rögner, M., Kruij, J., Schlodder, E., Karapetyan, N. V., Dekker, J. P., and van Grondelle, R. (2001) Time-Resolved Fluorescence Emission Measurements of Photosystem I Particles of Various Cyanobacteria: A Unified Compartmental Model. *Biophys. J.* 81, 407–424.
- Holzwarth, A. R., Müller, M. G., Niklas, J., and Lubitz, W. (2006) Ultrafast Transient Absorption Studies on Photosystem I Reaction Centers from *Chlamydomonas reinhardtii*. 2: Mutations near the P700 Reaction Center Chlorophylls Provide New Insight into the Nature of the Primary Electron Donor. *Biophys. J.* 90, 552–565.
- Kumazaki, S., Ikegami, I., Furusawa, H., Yasuda, S., and Yoshihara, K. (2001) Observation of the Excited State of the Primary Electron Donor Chlorophyll (P700) and the Ultrafast Charge Separation in the Spinach Photosystem I Reaction Center. *J. Phys. Chem. B* 105, 1093–1099.
- Slavov, C., El-Mohsnawy, E., Rögner, M., and Holzwarth, A. R. (2009) Trapping kinetics in isolated cyanobacterial PS I complexes. *Chem. Phys.* 357, 163–170.
- Vaswani, H. M., Stenger, J., Fromme, P., and Fleming, G. R. (2006) One- and Two-Color Photon Echo Peak Shift Studies of Photosystem I. *J. Phys. Chem. B* 110, 26303–26312.
- Müller, M. G., Niklas, J., Lubitz, W., and Holzwarth, A. R. (2003) Ultrafast Transient Absorption Studies on Photosystem I Reaction Centers from *Chlamydomonas reinhardtii*. 1. A New Interpretation of the Energy Trapping and Early Electron Transfer Steps in Photosystem I. *Biophys. J.* 85, 3899–3922.
- Gibasiewicz, K., Ramesh, V. M., Melkozernov, A. N., Lin, S., Woodbury, N. W., Blankenship, R. E., and Webber, A. N. (2001) Excitation Dynamics in the Core Antenna of PS I from *Chlamydomonas reinhardtii* CC 2696 at Room Temperature. *J. Phys. Chem. B* 105, 11498–11506.
- Melkozernov, A. N., Lin, S., and Blankenship, R. E. (2000) Excitation Dynamics and Heterogeneity of Energy Equilibration in the Core Antenna of Photosystem I from the Cyanobacterium *Synechocystis* sp. PCC 6803. *Biochemistry* 39, 1489–1498.
- Melkozernov, A. N., Schmid, V. H. R., Lin, S., Paulsen, H., and Blankenship, R. E. (2002) Excitation Energy Transfer in the Lhca1 Subunit of LHC I-730 Peripheral Antenna of Photosystem I. *J. Phys. Chem. B* 106, 4313–4317.
- Savikhin, S., Xu, W., Martinsson, P., Chitnis, P. R., and Struve, W. S. (2001) Kinetics of Charge Separation and A0 to A1 Electron Transfer in Photosystem I Reaction Centers. *Biochemistry* 40, 9282–9290.
- Gobets, B., van Stokkum, I. H. M., van Mourik, F., Dekker, J. P., and van Grondelle, R. (2003) Excitation Wavelength Dependence of the Fluorescence Kinetics in Photosystem I Particles from *Synechocystis* PCC 6803 and *Synechococcus elongatus*. *Biophys. J.* 85, 3883–3898.
- Croce, R., Dorra, D., Holzwarth, A. R., and Jennings, R. C. (2000) Fluorescence Decay and Spectral Evolution in Intact Photosystem I of Higher Plants. *Biochemistry* 39, 6341–6348.

28. Nabedryk, E., Allen, J. P., Taguchi, A. K. W., Williams, J. C., Woodbury, N. W., and Breton, J. (1993) Fourier transform infrared study of the primary electron donor in chromatophores of *Rhodobacter sphaeroides* with reaction centers genetically modified at residues M160 and L131. *Biochemistry* 32, 13879–13885.
29. Pawlowicz, N. P., van Grondelle, R., van Stokkum, I. H. M., Breton, J., Jones, M. R., and Groot, M. L. (2008) Identification of the First Steps in Charge Separation in Bacterial Photosynthetic Reaction Centers of *Rhodobacter sphaeroides* by Ultrafast Mid-Infrared Spectroscopy: Electron Transfer and Protein Dynamics. *Biophys. J.* 95, 1268–1284.
30. Maiti, S., Walker, G. C., Cowen, B. R., Pippenger, R., Moser, C. C., Dutton, P. L., and Hochstrasser, R. M. (1994) Femtosecond coherent transient infrared spectroscopy of reaction centers from *Rhodobacter sphaeroides*. *Proc. Natl. Acad. Sci. U.S.A.* 91, 10360–10364.
31. Hamm, P., and Zinth, W. (1995) Ultrafast initial reaction in bacterial photosynthesis revealed by femtosecond infrared spectroscopy. *J. Phys. Chem.* 99, 13537–13544.
32. Groot, M. L., Pawlowicz, N. P., van Wilderen, L. J. G. W., Breton, J., van Stokkum, I. H. M., and van Grondelle, R. (2005) Initial electron donor and acceptor in isolated Photosystem II reaction centers identified with femtosecond mid-IR spectroscopy. *Proc. Natl. Acad. Sci. U.S.A.* 102, 13087–13092.
33. Di Donato, M., Cohen, R. O., Diner, B. A., Breton, J., van Grondelle, R., and Groot, M. L. (2008) Primary Charge Separation in the Photosystem II Core from *Synechocystis*: A Comparison of Femtosecond Visible/Mid-infrared Pump-Probe Spectra of Wild-Type and Two P680 Mutants. *Biophys. J.* 94, 4783–4795.
34. Romero, E., Mozzo, M., van Stokkum, I. H. M., Dekker, J. P., van Grondelle, R., and Croce, R. (2009) The Origin of the Low-Energy Form of Photosystem I Light-Harvesting Complex Lhca4: Mixing of the Lowest Exciton with a Charge-Transfer State. *Biophys. J.* 96, L35–L37.
35. Frese, R. N., Palacios, M. A., Azzizi, A., van Stokkum, I. H. M., Kruij, J., Rogner, M., Karapetyan, N. V., Schlodder, E., van Grondelle, R., and Dekker, J. P. (2002) Electric field effects on red chlorophylls, β -carotenes and P700 in cyanobacterial Photosystem I complexes. *Biochim. Biophys. Acta* 1554, 180–191.
36. Giera, W., Ramesh, V. M., Webber, A. N., van Stokkum, I., van Grondelle, R., and Gibasiewicz, K. (2010) Effect of the P700 pre-oxidation and point mutations near A0 on the reversibility of the primary charge separation in Photosystem I from *Chlamydomonas reinhardtii*. *Biochim. Biophys. Acta* 1797, 106–112.
37. Fromme, P., and Witt, H. T. (1998) Improved isolation and crystallization of photosystem I for structural analysis. *Biochim. Biophys. Acta* 1365, 175–184.
38. van Stokkum, I. H. M., Larsen, D. S., and van Grondelle, R. (2004) Global and target analysis of time-resolved spectra. *Biochim. Biophys. Acta* 1657, 82–104.
39. Cross, G. L., Katz, J. J., Pennington, F. C., Thomas, M. R., and Strain, H. H. (1963) Nuclear Magnetic Resonance Spectra and Molecular Association of Chlorophylls a and b, Methyl Chlorophyllides, Pheophytins, and Methyl Pheophorbides. *J. Am. Chem. Soc.* 85, 3809–3821.
40. Groot, M. L., Breton, J., van Wilderen, L. J. G. W., Dekker, J. P., and van Grondelle, R. (2004) Femtosecond Visible/Visible and Visible/Mid-IR Pump-Probe Study of the Photosystem II Core Antenna Complex CP47. *J. Phys. Chem. B* 108, 8001–8006.
41. Di Donato, M., van Grondelle, R., van Stokkum, I. H. M., and Groot, M. L. (2007) Excitation Energy Transfer in the Photosystem II Core Antenna Complex CP43 Studied by Femtosecond Visible/Visible and Visible/Mid-Infrared Pump Probe Spectroscopy. *J. Phys. Chem. B* 111, 7345–7352.
42. Noguchi, T., Tomo, T., and Inoue, Y. (1998) Fourier Transform Infrared Study of the Cation Radical of P680 in the Photosystem II Reaction Center: Evidence for Charge Delocalization on the Chlorophyll Dimer. *Biochemistry* 37, 13614–13625.
43. Barth, A. (2007) Infrared spectroscopy of proteins. *Biochim. Biophys. Acta* 1767, 1073–1101.
44. Noguchi, T., Mitsuka, T., and Inoue, Y. (1994) Fourier transform infrared spectrum of the radical cation of β -carotene photoinduced in photosystem II. *FEBS Lett.* 356, 179–182.
45. Mantele, W. G., Wollenweber, A. M., Nabedryk, E., and Breton, J. (1988) Infrared spectroelectrochemistry of bacteriochlorophylls and bacteriopheophytins: Implications for the binding of the pigments in the reaction center from photosynthetic bacteria. *Proc. Natl. Acad. Sci. U.S.A.* 85, 8468–8472.
46. Hartwich, G., Geskes, C., Scheer, H., Heinze, J., and Maentele, W. (1995) Fourier transform infrared spectroscopy of electrogenerated anions and cations of metal-substituted bacteriochlorophyll a. *J. Am. Chem. Soc.* 117, 7784–7790.
47. Shelaev, I. V., Gostev, F. E., Mamedov, M. D., Sarkisov, O. M., Nadochenko, V. A., Shuvalov, V. A., and Semenov, A. Y. (2010) Femtosecond primary charge separation in *Synechocystis* sp. PCC 6803 photosystem I. *Biochim. Biophys. Acta* 1797, 1410–1420.
48. Nabedryk, E., Robles, S. J., Goldman, E., Youvan, D. C., and Breton, J. (1992) Probing the primary donor environment in the histidineM200 to leucine and histidineL173 to leucine heterodimer mutants of *Rhodobacter capsulatus* by light-induced Fourier transform infrared difference spectroscopy. *Biochemistry* 31, 10852–10858.
49. Pawlowicz, N. P., Groot, M. L., van Stokkum, I. H. M., Breton, J., and van Grondelle, R. (2007) Charge Separation and Energy Transfer in the Photosystem II Core Complex Studied by Femtosecond Mid-infrared Spectroscopy. *Biophys. J.* 93, 2732–2742.
50. Groot, M. L., Peterman, E. J., van Kan, P. J., van Stokkum, I. H., Dekker, J. P., and van Grondelle, R. (1994) Temperature-dependent triplet and fluorescence quantum yields of the photosystem II reaction center described in a thermodynamic model. *Biophys. J.* 67, 318–330.
51. Woodbury, N. W. T., and Parson, W. W. (1984) Nanosecond fluorescence from isolated photosynthetic reaction centers of *Rhodospseudomonas sphaeroides*. *Biochim. Biophys. Acta* 767, 345–361.
52. Breton, J. (2001) Fourier transform infrared spectroscopy of primary electron donors in type I photosynthetic reaction centers. *Biochim. Biophys. Acta* 1507, 180–193.
53. Palsson, L.-O., Flemming, C., Gobets, B., van Grondelle, R., Dekker, J. P., and Schlodder, E. (1998) Energy Transfer and Charge Separation in Photosystem I: P700 Oxidation Upon Selective Excitation of the Long-Wavelength Antenna Chlorophylls of *Synechococcus elongatus*. *Biophys. J.* 74, 2611–2622.
54. de Weerd, F. L., Dekker, J. P., and van Grondelle, R. (2003) Dynamics of β -Carotene-to-Chlorophyll Singlet Energy Transfer in the Core of Photosystem II. *J. Phys. Chem. B* 107, 6214–6220.
55. de Weerd, F. L., Kennis, J. T. M., Dekker, J. P., and van Grondelle, R. (2003) β -Carotene to Chlorophyll Singlet Energy Transfer in the Photosystem I Core of *Synechococcus elongatus* Proceeds via the β -Carotene S2 and S1 States. *J. Phys. Chem. B* 107, 5995–6002.
56. Croce, R., Chojnicka, A., Morosinotto, T., Ihalainen, J. A., van Mourik, F., Dekker, J. P., Bassi, R., and van Grondelle, R. (2007) The Low-Energy Forms of Photosystem I Light-Harvesting Complexes: Spectroscopic Properties and Pigment-Pigment Interaction Characteristics. *Biophys. J.* 93, 2418–2428.
57. Sytina, O. A., van Stokkum, I. H. M., Heyes, D. J., Hunter, C. N., van Grondelle, R., and Groot, M. L. (2010) Protochlorophyllide Excited-State Dynamics in Organic Solvents Studied by Time-Resolved Visible and Mid-Infrared Spectroscopy. *J. Phys. Chem. B* 114, 4335–4344.
58. Wilson, A. L., Punginelli, C., Gall, A., Bonetti, C., Alexandre, M., Routaboul, J.-M., Kerfeld, C. A., van Grondelle, R., Robert, B., Kennis, J. T. M., and Kirilovsky, D. (2008) A photoactive carotenoid protein acting as light intensity sensor. *Proc. Natl. Acad. Sci. U.S.A.* 105, 12075–12080.
59. Hughes, J. L., Smith, P., Pace, R., and Krausz, E. (2006) Charge separation in photosystem II core complexes induced by 690–730 nm excitation at 1.7 K. *Biochim. Biophys. Acta* 1757, 841–851.
60. Van Brederode, M. E., Jones, M. R., Van Mourik, F., Van Stokkum, I. H. M., and Van Grondelle, R. (1997) A New Pathway for Transmembrane Electron Transfer in Photosynthetic Reaction Centers of *Rhodobacter sphaeroides* Not Involving the Excited Special Pair. *Biochemistry* 36, 6855–6861.
61. van Brederode, M. E., van Mourik, F., van Stokkum, I. H. M., Jones, M. R., and van Grondelle, R. (1999) Multiple pathways for ultrafast transduction of light energy in the photosynthetic reaction center of *Rhodobacter sphaeroides*. *Proc. Natl. Acad. Sci. U.S.A.* 96, 2054–2059.
62. Holzwarth, A. R., Müller, M. G., Reus, M., Nowaczyk, M., Sander, J., and Ragner, M. (2006) Kinetics and mechanism of electron transfer in intact photosystem II and in the isolated reaction center: Pheophytin is the primary electron acceptor. *Proc. Natl. Acad. Sci. U.S.A.* 103, 6895–6900.
63. Sivakumar, V., Wang, R., and Hastings, G. (2005) A1 Reduction in Intact Cyanobacterial Photosystem I Particles Studied by Time-Resolved Step-Scan Fourier Transform Infrared Difference Spectroscopy and Isotope Labeling. *Biochemistry* 44, 1880–1893.
64. Groot, M. L., Pawlowicz, N. P., van Wilderen, L. J. G. W., Breton, J., van Stokkum, I. H. M., and van Grondelle, R. (2005) Initial electron donor and acceptor in isolated Photosystem II reaction centers identified with femtosecond mid-IR spectroscopy. *Proc. Natl. Acad. Sci. U.S.A.* 102, 13087–13092.

65. Burie, J.-R., Boussac, A., Boullais, C., Berger, G., Mattioli, T., Mioskowski, C., Nbedryk, E., and Breton, J. (1995) FTIR Spectroscopy of UV-Generated Quinone Radicals: Evidence for an Intramolecular Hydrogen Atom Transfer in Ubiquinone, Naphthoquinone, and Plastoquinone. *J. Phys. Chem.* *99*, 4059–4070.
66. Breton, J., Burie, J.-R., Berthomieu, C., Berger, G., and Nbedryk, E. (1994) The Binding Sites of Quinones in Photosynthetic Bacterial Reaction Centers Investigated by Light-Induced FTIR Difference Spectroscopy: Assignment of the QA Vibrations in *Rhodobacter sphaeroides* Using ¹⁸O- or ¹³C-Labeled Ubiquinones and Vitamin K1. *Biochemistry* *33*, 4953–4965.
67. Renger, T., and Schlodder, E. (2010) Primary Photophysical Processes in Photosystem II: Bridging the Gap between Crystal Structure and Optical Spectra. *ChemPhysChem* *11*, 1141–1153.